Journal of
Synchrotron Radiation

ISSN 0909-0495

Received 22 October 2008
Accepted 30 January 2009

Development of new apertures for coherent X-ray experiments

Eric M. Dufresne,[a]*‡ Steven B. Dierker,[b]‡ Z. Yin[b] and Lonny Berman[b]

[a]The Advanced Photon Source, Argonne National Laboratory, Argonne, IL 60439, USA, and [b]The National Synchrotron Light Source, Brookhaven National Laboratory, Upton, NY 11973, USA. E-mail: dufresne@anl.gov

When one performs a coherent small-angle X-ray scattering experiment, the incident beam must be spatially filtered by slits on a length scale smaller than the transverse coherence length of the source which is typically around 10 μm. The Fraunhofer diffraction pattern of the slit is one of the important sources of background in these experiments. New slits which minimize this parasitic background have been designed and tested. The slit configuration apodizes the beam by the use of partially transmitting inclined slit jaws. A model is presented which predicts that the high wavevector tails of the diffraction pattern fall as the inverse fourth power of the wavevector instead of the inverse second power that is observed for standard slits. Using cleaved GaAs single-crystal edges, Fraunhofer diffraction patterns from 3 and 5.5 keV X-rays were measured, in agreement with the theoretical model proposed. A novel phase-peak diffraction pattern associated with phase variations of the transmitted electric field was also observed. The model proposed adequately accounts for this phenomenon.

Keywords: XPCS; SAXS; Fraunhofer diffraction; coherence.

1. Introduction

In a small-angle X-ray scattering (SAXS) experiment, one may be sensitive to parasitic scattering from the imperfections of beamline optical components. The apertures used to limit the illuminated sample volume and collimate the beam can become one of the important sources of parasitic background in the far-field diffraction plane. The imperfections of the edges cause random scattering and the finite opening of the aperture diffracts the X-rays. This is particularly important when performing a SAXS experiment with X-ray photon correlation spectroscopy (XPCS) (Dierker *et al.*, 1995), especially when the scattering from the sample is weak and at low wavevectors (Dufresne *et al.*, 2002) (for a recent review of XPCS, see Livet, 2007). For example, when observing critical fluctuations in a binary fluid mixture, it was important to reduce the background from parasitic scattering near $q = 0$ (Dufresne *et al.*, 2002). The transverse coherence of a light source is characterized by a transverse coherence length, $l_t = \lambda R/d$, where λ is the X-ray wavelength, R is the source–experiment distance and d is the source size (Goodman, 1985). For a wavelength $\lambda = 4.0$ Å, a distance $R = 20$ m and a horizontal source size $d = 600$ μm, the transverse coherence length is $l_t = 13$ μm. By limiting the illuminated sample area to linear dimensions smaller than l_t, the sample can be illuminated with a beam of coherent X-rays. This has been done in the past with small pinholes, made by laser drilling of a thin Pt foil. The far-field diffracted intensity of a circular pinhole with a radius r is $I(q) \propto [J_1(qr)/(qr)]^2$ (Goodman, 1985). For large wavevectors, since $J_1^2(qr) \propto 1/q$, $I(q)$ decreases as q^{-3}. In comparison, a one-dimensional slit has q^{-2} tails, since the intensity follows $I(q) \propto [\sin(q\Delta/2)/(q\Delta/2)]^2$, where Δ is the slit opening. Circular pinholes were first used in XPCS (Dierker *et al.*, 1995; Brauer *et al.*, 1995). The advantage of using pinholes is that they are relatively convenient to align, and their tails fall more sharply than a one-dimensional slit. On the other hand, they are produced by laser ablation of a thin metallic foil, which cannot control the shape of the hole accurately, and their diameter is fixed. Fig. 1 shows a typical diffraction pattern for a typical 10 μm pinhole. The beam was filtered with a pair of WB_4C multilayers with a 27 Å period and a 1.5% bandwidth (Berman *et al.*, 1997). Their diffraction pattern is typically non-symmetric, showing large flares and long tails, thus the decay of their tails is not easy to control. Recently, a casting method has also been used to make these small pinholes but their diffraction pattern still remained irregular (van der Veen *et al.*, 1997). It has been shown recently that pinholes made for electron microscopy work well, so it is possible to overcome fabrication difficulties (Livet, 2007).

Rectangular apertures made with either a roller-blade design (Libbert *et al.*, 1997) or with highly polished tungsten edges (Vlieg *et al.*, 1997) have been shown to produce well controlled diffraction patterns. They are now the method of choice for coherent illumination of a sample. One of the

‡ Formerly at the Department of Physics, University of Michigan, Ann Arbor, MI 48109, USA.

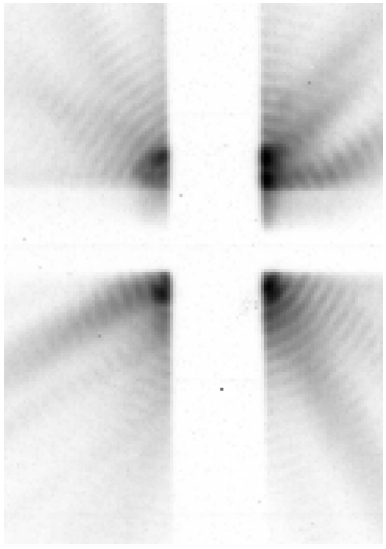

Figure 1
Diffraction pattern of a circular 10 µm-diameter pinhole generated with 3.1 keV X-rays and measured with a CCD having 9 µm pixels, placed approximately 1 m from the pinhole. The logarithmic grey scale uses black as the high intensity. The beam stop (a cross) is used to extend the dynamic range in the tails of the diffraction pattern.

advantage of using slits is that their opening is variable, so they can be set easily to match the smallest transverse coherence length in the experiment, or easily closed to increase the limiting wavevector q_l, where the speckle contrast is reduced owing to the loss of longitudinal coherence (see §3). An important gain in parasitic background reduction can be made by using a square aperture if one chooses a scattering direction which is along the diagonal of the square, pointing 45° from any of the edges. The tails then fall off as q^{-4}, *i.e.* faster than for a circular aperture. If smooth polished edges are made, then an important reduction in parasitic background from the aperture diffraction pattern can be achieved.

For coherent small-angle X-ray scattering, one typically reduces the parasitic scattering from the slit blades by setting up a guard aperture downstream of the coherence slit (Livet, 2007). One would typically set the guard aperture within the near-field of the coherence slit, with an opening larger than the coherence slit. Another recent approach reduces the parasitic background by adding a channel-cut monochromator between the guard slit and the sample (Xiao *et al.*, 2006). This novel approach reduces the background more than with only a guard slit.

In this paper we will describe a new technique which can reduce the parasitic diffraction more than a 45° geometry. The idea is based on the technique of apodization in optics (Born & Wolf, 1970). By making a soft transmitting edge where the intensity varies gradually over some distance, one can reduce the amplitudes of the Fourier components at high wavevectors. Such an edge is shown in Fig. 2. This figure shows how, by using an inclined slit jaw, one can produce an intensity profile in a plane behind the aperture where the intensity decreases more slowly along the *x*-direction than for an opaque slit jaw. We chose to investigate an exponential profile in the jaw because it was simpler to make such a jaw experimentally, but

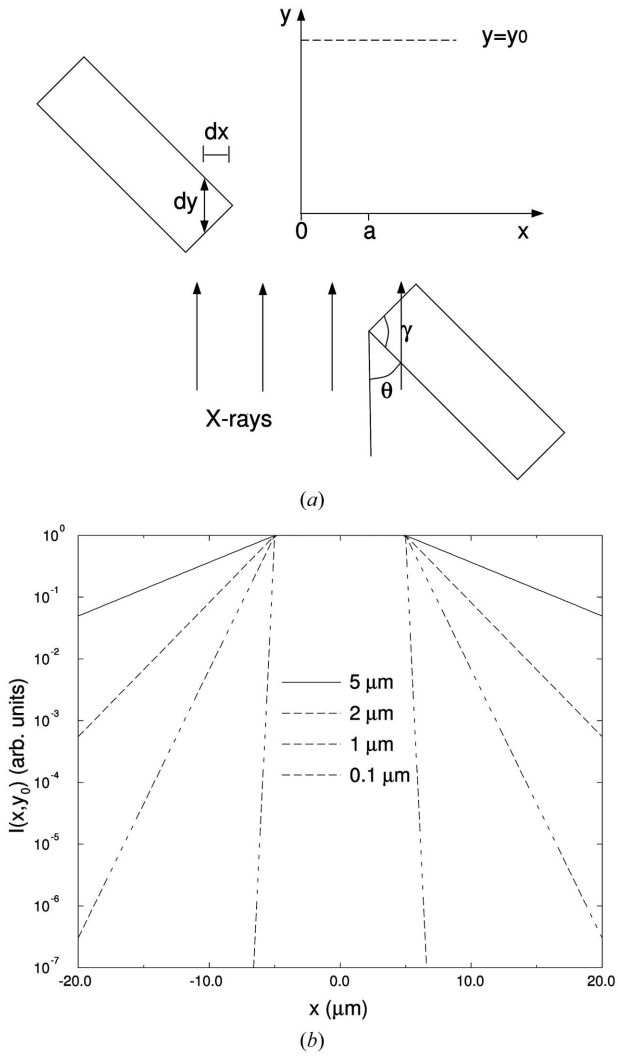

Figure 2
(*a*) The slits geometry and its coordinate system. The beam propagates along *y*. (*b*) Theoretical intensity profile $I(x,y_0)$ in the near-field diffraction region for several effective absorption lengths.

clearly other geometries could be further investigated (Libbert *et al.*, 1997). Although refraction effects from the edges of slits have been discussed recently, they were measured using a laboratory source with incoherent X-rays (Nikulin & Davis, 1998). This paper gives a detailed theory of the effect where diffraction and refraction effects from coherent X-rays are included. We will show in §2 that the tails of the diffracted intensity falls as q^{-4} along the *x*-axis, a substantial improvement over a circular aperture. The experimental method and the results sections will describe the first observation of a peculiar phase grating diffraction pattern. Finally, we will discuss the implications of these observations for coherent and incoherent small-angle scattering experiments.

2. Theory: X-ray phase grating aperture

Fig. 2 shows a one-dimensional slit. To prevent the jaws from colliding, we purposefully offset the slit jaw planes of motion.

Table 1
Phase peak position *versus* θ for 3 and 8 keV X-rays in GaAs.

The phase peak position increases with increasing θ. At 3 and 8 keV the magnitude of k_p is in the range where one would typically observe small-angle scattering. For constant α, $k_p(3\text{ keV}) > k_p(8\text{ keV})$, as expected from the wavelength dependence of k_p.

θ (°)	α	k_p at 3 keV (Å^{-1})	k_p at 8 keV (Å^{-1})
45	2.0	3.3×10^{-4}	1.2×10^{-4}
60	2.3	3.8×10^{-4}	1.4×10^{-4}
80	5.8	9.7×10^{-4}	3.3×10^{-4}
85	11.5	1.9×10^{-3}	6.8×10^{-4}
89	57.3	9.5×10^{-3}	3.4×10^{-3}

Two perpendicular slit assemblies can be placed one after the other to define a two-dimensional aperture. We assume that linearly polarized X-rays are incident on the slits. This condition is a good approximation for synchrotron radiation, especially for radiation emitted by an undulator. For experimental considerations, the wedge angle $\gamma = 90°$ because our GaAs blades cleaved well for this cleavage plane. As shown in Fig. 2, the path length in the slit material along the beam direction is $\mathrm{d}y = \alpha\,\mathrm{d}x$, where $\alpha = \tan\theta + 1/\tan\theta = 2/\sin(2\theta)$. The function $\alpha(\theta)$ has a minimum at $\theta = \pi/4$, where $\alpha = 2$, and diverges when $\theta \rightarrow \pi/2$ or $\theta \rightarrow 0$, making the slit jaws opaque. Several values of α are given in Table 1. To produce a more slowly decreasing intensity profile, one could choose a wedge with an angle $\gamma < 90°$. In that case, one would replace the inclination coefficient by $\alpha = \tan^{-1}(\theta) - \tan^{-1}(\theta + \gamma)$. To simplify the theoretical treatment, we assume that the inclination angles of the two edges are identical. The slit blades are positioned at $x = \pm a$, thus the opening of the slit is $\Delta = 2a$. Assuming that a plane wave is incident with wavevector $\mathbf{k} = k_0 y$, where $k_0 = 2\pi/\lambda$, the field just behind the slit in the near field diffraction region at $y = y_0 \ll \Delta^2/\lambda$ is

$$E(x) = \begin{cases} E_0 & \text{for } |x| < a, \\ E_0 \exp[i(n-1)k_0\alpha\,\mathrm{d}x] & \text{for } |x| > a. \end{cases} \quad (1)$$

Here, E_0 is the incident electric field amplitude and we neglected any constant phase factor in deriving $E(x)$. The horizontal distance with respect to a given edge is $\mathrm{d}x = x - a$ for $x > a$, and $\mathrm{d}x = -x - a$ for $x < -a$. For X-rays, the index of refraction $n = 1 - \delta + i\beta$, where δ is the index of refraction decrement, and β is the absorption coefficient. Some values of δ and β for GaAs are shown in Table 2. As opposed to visible light, X-ray photons have an index of refraction slightly lower than unity, and the absorption correction is typically smaller than the refraction correction. A surprising aspect of these slits is that they still define an aperture, even when the two jaws overlap. The electric field when the slit is closed is similar to the previous equation, apart from a multiplicative factor $\exp[ik_0(n-1)\alpha 2|a|]$, where a here is negative. This factor comes from the fact that, when the slit is closed, the path length difference through the overlapping edges is a constant equal to $2\alpha|a|$ for $|x| < |a|$.

By inspecting the previous equation for $|x| > a$, one notices that the phase of the electric field varies with a wavevector $k_p = k_0\alpha\delta$ along the x-axis. From this periodic variation, one can expect a peak in the diffraction pattern at k_p. For later discussions, let us define the effective slit opening $\Delta_{\text{eff}} = \Delta + 1/(g\beta)$, where $(2g\beta)^{-1}$ is the distance from $x = \pm a$ where $|E(x)|^2$ falls by a factor $1/e$ and $g = \alpha k_0$. Some typical values of Δ_{eff} with $\Delta = 0$ are shown in Table 2 for GaAs. The effective slit opening increases with energy. To observe good fringe contrast in a Fraunhofer diffraction pattern, the effective opening must be smaller than the smallest of the transverse coherence lengths. GaAs is best as a jaw material near 3 keV because the contribution of the jaws $1/(g\beta)$ is smaller than the typical physical slit opening $\Delta \simeq 10$ µm, thus the slit can be set to match the transverse coherence condition. In principle, GaAs could be used at higher energies by increasing g, setting the inclination angle θ near 90°. In practice, it may be easier to select a more absorbing material than to precisely align θ. Recently, we have used GaAs near 11.0 keV with $\theta \simeq 0°$ just below the Ga and As absorption edges. The large absorption just below the edge is sufficient to make the edges opaque enough for a standard slit (Dufresne *et al.*, 2002).

Table 2
Typical values of δ and β at several energies for GaAs (from Henke *et al.*, 1993).

The effective slit opening $\Delta_{\text{eff}} = \Delta + 1/(g\beta)$ is also shown at several energies for $\theta = 60°$ and for a slit opening $\Delta = 0$ µm. GaAs slit jaws work well at 3 keV.

Energy (keV)	δ	β	Δ_{eff}
3	1.1×10^{-4}	1.7×10^{-5}	1.7
4	6.1×10^{-5}	5.9×10^{-6}	3.6
6	2.7×10^{-5}	1.3×10^{-6}	11
8	1.5×10^{-5}	4.5×10^{-7}	24
10	9.1×10^{-6}	1.9×10^{-7}	45

The electric field in the far-field diffraction plane is the Fourier transform of $E(x)$. Defining the Fourier transform of $E(x)$ as $E(k) = \int \exp(ikx)E(x)\,\mathrm{d}x$, one can show that

$$E(k) = E_0 \frac{2g(\beta + i\delta)}{k^2 + g^2(\beta^2 - \delta^2) + i2g^2\beta\delta} \times \left[g\frac{\beta + i\delta}{k}\sin(ka) + \cos(ka) \right]. \quad (2)$$

For infinite absorption when $\beta \rightarrow \infty$, the previous equation yields the same results as a simple one-dimensional slit with $E(k) \propto \sin(ka)/(ka)$. The field is also proportional to $\sin(ka)/(ka)$ when $\theta \rightarrow \pi/2$ or $\theta \rightarrow 0$ since $g \rightarrow \infty$. It is interesting to note that $E(k)$ is quite similar to the form factor of a blazed transmission grating (Michette & Buckley, 1993). Recalling that the intensity is just $I(k) = |E(k)|^2$, one finds that

$$I(k)/I_0 = \frac{4g^2(\beta^2 + \delta^2)}{[k^2 + g^2(\beta^2 - \delta^2)]^2 + 4g^4\beta^2\delta^2} \times \left[g^2(\beta^2 + \delta^2)\frac{\sin^2(ka)}{k^2} + \cos^2(ka) + g\beta\frac{\sin(2ka)}{k} \right], \quad (3)$$

where $I_0 = {E_0}^2$. A similar equation can be derived easily when the slit is closed. It differs from the previous equation by only a numerical factor $\exp(-4g\beta|a|)$.

Setting $a = 0$ in equation (3), $I(k)$ is maximized when $k^2 + g^2(\beta^2 - \delta^2) = 0$, thus the phase peak wavevector is $k_p =$

$\pm g(\delta^2 - \beta^2)^{1/2}$. Since typically $\delta \gg \beta$ for hard X-rays, $k_p \simeq \pm g\delta$. Note that a phase peak would be absent if $\delta < \beta$. This situation typically occurs in materials in the ultraviolet and the soft X-ray energies (Henke *et al.*, 1993). The phase peak is a simple refraction effect whose position can be estimated easily from the symmetric prism formula with the deflection angle between the main beam and refracted beam $\varphi = 2\delta\tan(\gamma/2)$, with $\theta = \pi/2 - \gamma/2$ (Born & Wolf, 1970). In our case, the prism angle $\gamma = \pi/2$, and $\theta = \pi/4$, thus $\varphi = 2\delta$. For $\theta = \pi/4$, the inclination parameter $\alpha = 2$, $k_p = 2\delta k_0$, thus the deflection angle is also 2δ.

The half width at half-maximum of this peak occurs when $k^2 + g^2(\beta^2 - \delta^2) = \pm 2g^2\beta\delta$. The full width at half-maximum (FWHM) of the phase peak is $\Delta k = g(\delta^2 - \beta^2 + 2\beta\delta)^{1/2} - g(\delta^2 - \beta^2 - 2\beta\delta)^{1/2} \simeq 2g\beta$, when $\delta \gg \beta$. By inspection, the previous equation falls as $I(k) \rightarrow k^{-4}$, for $|k - k_p| \gg 2g\beta$. Since β and δ are typically around 10^{-5} (see Table 2), and g ranges between 1 and 10 Å^{-1}, $I(k)$ will fall as k^{-4} in the range of interest for a small-angle scattering experiment (>10^{-4} Å^{-1}). For finite a and small $k \rightarrow 0$, the $\sin^2(ka)/k^2$ term dominates in equation (3).

In Figs. 3 and 4 we show the behavior of equation (3) for GaAs edges illuminated with 3 keV X-rays. Fig. 3 shows $I(q)$ for several slit openings $\Delta = 2a$. In Figs. 3–5, we normalized $I(k)$ so that $\int I(k)\,dk = I_0$. Perhaps the most surprising aspect of this figure is the fact that a peak is observed, away from $q = 0$, even when the slits are closed. This peak remains fixed in reciprocal space as the opening is increased. This is the phase peak, centered around $k_p = 3.8 \times 10^{-4}$ Å^{-1}, in agreement with the computed value in Table 1. For wavevectors much larger than k_p, $I(k) \simeq k^{-4}$ as discussed earlier. As expected, the periodicity of the fringes in reciprocal space also increases as the slit opening is increased.

Fig. 4 shows the diffracted intensity for a fixed opening Δ = 5 µm illuminated with X-rays, for various inclination angles θ. As θ is increased, the phase peak moves to higher wavevectors

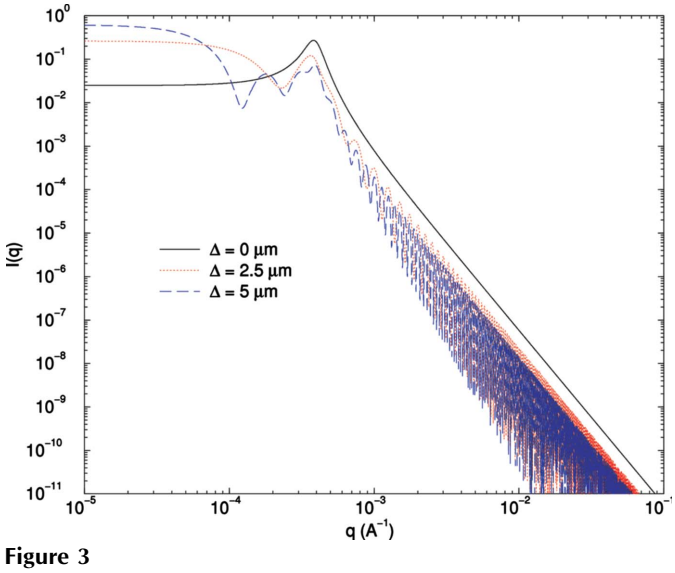

Figure 3
Calculated diffracted intensity $I(q)$ for several openings $\Delta = 2a$ at 3 keV using GaAs edges with $\theta = 60°$.

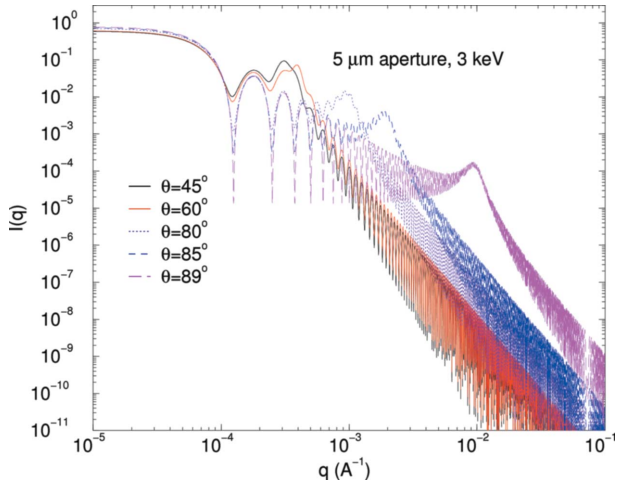

Figure 4
Diffracted intensity $I(q)$ for a fixed opening Δ = 5 µm for several values of θ. Increasing the inclination angle moves the phase peak at larger wavevector.

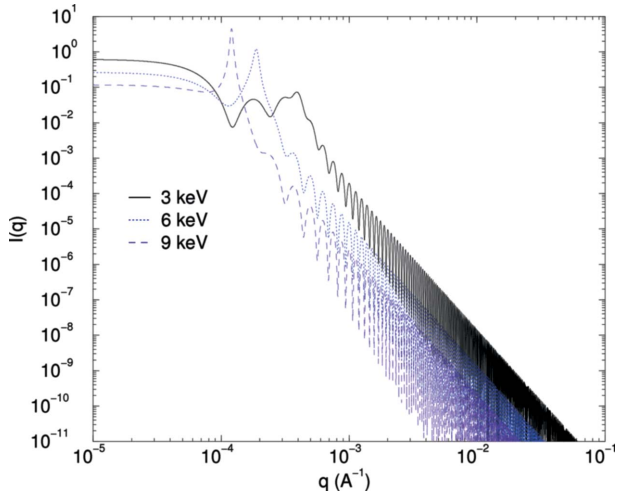

Figure 5
Diffracted intensity $I(q)$ for three different energies with a 5 µm aperture and $\theta = 60°$. The phase peak wavevector is inversely proportional to energy.

and more diffracted intensity is found at higher wavevectors near 10^{-3} Å^{-1}. Since $k_p = k_0\alpha\delta$, this peak moves to higher wavevector when θ increases since $d\alpha/d\theta > 0$ for $\pi/4 < \theta < \pi/2$. This dependence is shown in Table 1 for several values of α. The positions of the phase peak in Fig. 4 agree with the values calculated in Table 1 for 3 keV X-rays. Note that, for $\theta = 89°$, the diffracted pattern for small wavevector ($q < 10^{-2}$ Å^{-1}) becomes closer to $\sin^2(ka)/k^2$.

Fig. 5 shows the calculated intensity for several energies at fixed opening Δ and fixed θ. The position of the phase peak moves to lower wavevectors as the energy is increased. This is expected for X-rays given that $\delta \propto \lambda^2$ (Michette & Buckley, 1993), thus $k_p = (2\pi/\lambda)\alpha\delta \propto \lambda$. Some values of k_p are shown in Table 1 for GaAs at 3 and 8 keV. In Fig. 5, the intensity of the phase peak becomes higher than the intensity of the direct beam $I(k = 0)$ for 6 and 9 keV X-rays. This is due to the fact that at higher energies the contribution of the electric field

transmitted through the edges becomes the dominant contribution to the intensity since the total penetration length in the jaw material $1/(g\beta)$ is greater than the physical opening Δ. Since the transmitted field is modulated by a wavevector k_p, the intensity of the phase peak increases with respect to the intensity of the direct beam.

3. Experimental method

We used 400 µm-thick (100) GaAs wafers to make well controlled slit jaws. Their thickness was about 208 absorption lengths at 3 keV. It is well known that GaAs (100) wafers cleave easily, with atomically flat edge. By cleaving the GaAs wafer along a preferred axis, one can obtain almost ideal atomically flat jaws, without any need for polishing the jaw material with a fine grit. The slit design is shown in Fig. 6. The GaAs blades are clamped on a rotating mount by small set screws. The slits can be oriented easily to a given angle θ by rotating the mount. We set the angle θ with a protractor. We aligned each jaw carefully so that the edges were parallel with respect to each other. The jaw pivoting mount is attached to a bracket which slides on a small precision ball slide (see Appendix *A*). The slits are moved by DC motors which are coupled to the bracket by a 0–80 lead screw. The DC motors were controlled by a MM3000 controller, from Newport Corp. Recently, we have also controlled these motors with an OMS 8S VME card running under EPICS. The slit jaw positions are measured by standard encoders attached to the shaft of the DC motor. We found that a minimum backlash of 0.2 mm was necessary to insure that the positioning of the slits would be reproducible. The backlash was set at 0.3 mm on all slits. We believe that this backlash may have been caused by some play in the shaft of the DC motors (See Appendix *A*).

Fig. 7 shows the experimental set-up. We performed the experiment using the prototype small gap undulator (PSGU) at beamline X13 of the National Synchrotron Light Source (Stefan *et al.*, 1995). The fundamental of the PSGU undulator was set at 3.1 keV. Owing to the large absorption at 3.1 keV,

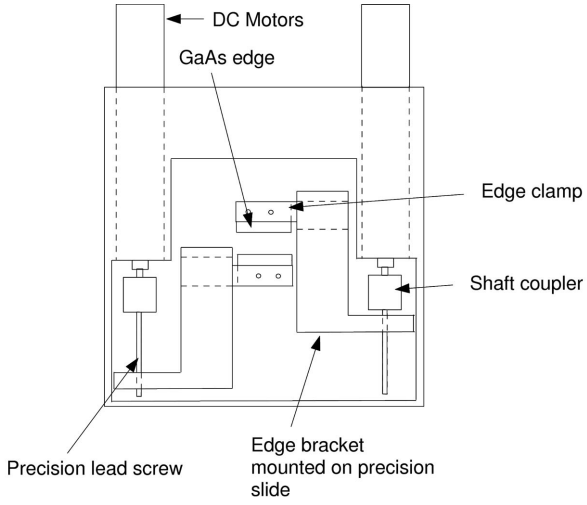

Figure 6
Schematic of the slit assembly.

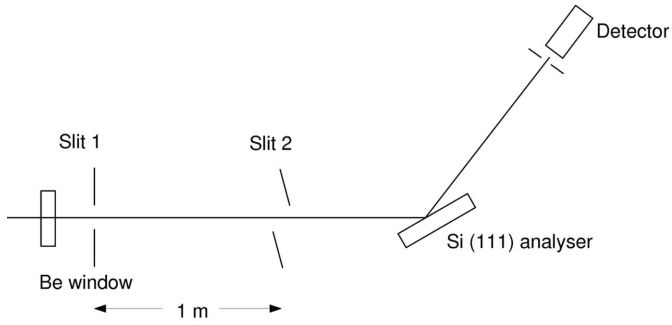

Figure 7
Experimental set-up.

the experiment was enclosed in a large plexiglass enclosure filled with He. The He enclosure and machine vacuum were isolated by a standard 250 µm-thick Be window, masked by a 80 µm-diameter pinhole, placed in contact with the window. The white beam was filtered with either a pair of vertically deflecting SiO_2 flat mirrors or a pair of WB_4C multilayer monochromators which filtered the higher harmonics.

The first slit, slit 1 in Fig. 7, was placed 4 cm behind the Be window. This two-dimensional aperture is made with two perpendicular PS-10X motor units from Newport Corp., using straight GaAs edges with $\theta = 90^\circ$. Placed approximately 1 m behind slit 1, slit 2 is defined with inclined GaAs edges that generate the Fraunhofer diffraction pattern. The inclination angles of the jaws were all set at $\theta \simeq 60^\circ$.

A Si (111) analyzer was used to generate the longitudinal coherence sufficient to observe good fringe visibility over a large range of angles in the detector plane. This analyzer selected a bandpass of about 0.5 eV out of the $\sim$100 eV pink beam. The Si analyzer crystal surface had a mirror finish, and did not affect the diffraction pattern. The longitudinal coherence is characterized by a longitudinal coherence length $l_l = \lambda/B$, where $B = \delta\lambda/\lambda$ is the relative bandwidth of the source (Goodman, 1985). This length scale depends on the choice of monochromator used in the experiment. For 3.1 keV X-rays diffracted with a Si (111) monochromator, the bandwidth $B = 1.4 \times 10^{-4}$, thus $l_l = 2.9$ µm. One can show that the fringe contrast will decrease when the path length difference $D\varphi > l_l$, where D is the diameter of the aperture used to limit the beam to its smallest transverse coherence length, and φ is the angle between the direct beam and the diffracted beam (Dierker, 1997). The first term in the previous relation comes from the path difference between two rays emitted from opposite sides of the aperture. Since the wavevector $q = 4\pi\sin(\varphi/2)/\lambda$, for small angles, the limiting wavector is $q_l \simeq 2\pi l_l/(\lambda D) = 0.91$ Å^{-1}, for $\lambda = 4.0$ Å and $D = 5$ µm.

Two detectors were used: a Si PIN diode, masked with a two-dimensional aperture, or a CCD directly exposed to X-rays. The PIN diode is the XR-100 from Amptek. A fast Canberra AFT amplifier was used to increase the dynamic range of the detector. The detected signal from the PIN diode was corrected for non-linearities with a dead-time correction. A two-dimensional aperture placed in front of the PIN diode and made with inclined edges defined the angular resolution

of the detector. The CCD was described in detail earlier (Dierker *et al.*, 1995). It uses a Kodak KAF-1400 CCD with 9 μm square pixels. The CCD is directly exposed to X-rays. To reduce the absorption at 3.1 keV from a Be window, we took it off and shielded any stray light from coming into the room. The two detectors were mounted on a horizontal translation stage which was itself installed on the 2θ arm of the Huber two-circle goniometer. Scanning the angle 2θ moved the detectors vertically.

4. Results

Fig. 8 shows the transmitted intensity through a two-dimensional aperture as a function of the opening in one dimension. We set the slit orientation angle θ for this calibration approximately to 60°. This figure shows our typical method for calibrating the slit jaw positions with the encoder readings of the controller. For example, with the vertical slit opened to 100 μm, we first position one of the horizontal edges in the center of the X-ray beam. Then we scan the other edge position and record the transmitted intensity with an ion chamber or the PIN diode. As expected in Fig. 8, the intensity follows an exponential when the slit is closed, and becomes linear when the slit is open. Note that the transmission when $\Delta = 0$ μm is quite large even for a closed slit. The solid line is a least-squares fit to the data. The theoretical curve for an opening Δ is

$$I(\Delta) = I_0[-\Delta + 1/(g\beta)]\exp(2g\beta\Delta) \qquad \text{for } \Delta < 0, \qquad (4)$$

$$I(\Delta) = I_0[\Delta + 1/(g\beta)] = I_0\Delta_{\text{eff}} \qquad \text{for } \Delta > 0. \qquad (5)$$

Here, $I(\Delta) = \int |E(x)|^2 \mathrm{d}x$, where $\Delta = 2a$ in equation (1). The fit is quite good, which shows that GaAs edges work well as weakly transmitting edges near 3 keV. The slope of the exponential in Fig. 8 is $2g\beta = 1.9\ \mu\text{m}^{-1}$. Recalling that $g = \alpha k_0 = 2k_0/\sin(2\theta)$, and using values of β in Table 1 at 3.1 keV, we find $\theta = 74°$. The difference between the angle obtained from the slope of Fig. 8 and the angle that we estimated the slits was set at could indicate misalignment of the slits assembly with respect to the incident beam. As shown in Fig. 8, the transmitted intensity measured by an ion chamber is proportional to the slit opening Δ for $\Delta > 0$. We scanned one of the edges six times (not shown). The calibration curve is reproducible to within ± 0.3 μm, thus the slit opening is reproducible within this limit.

Fig. 9 shows the Fraunhofer diffraction pattern of a nominal 6 μm × 6 μm aperture measured with the CCD. Slit 1 in Fig. 7 was closed to 5 μm × 5 μm. Here q_x is in the horizontal direction where the transverse coherence is the shortest. The image is displayed with a logarithmic grey scale. It is over-exposed in the center to enhance the dynamic range in the tails. This causes the long horizontal tail in the image. The diffraction pattern is symmetrical and quite regular. This aperture gives a very controlled diffraction pattern when compared with the pattern displayed in Fig. 1. No flares are observed. The diffraction from the edges here is also quite different than the usual diffraction pattern from a rectangular aperture. For example, the first fringes away from the main beam along $q_x = 0\ \text{Å}^{-1}$ have less intensity than the next fringes. The phase peak is near $0.4 \times 10^{-2}\ \text{nm}^{-1}$. The fringe visibility is also quite large. The intensity falls off rapidly to match the CCD readout noise which indicates that the apodization is reducing the intensity in the tails of the diffraction pattern. We found that the fringe visibility varied greatly by changing the opening of slit 1. The horizontal visibility of the fringes varied significantly when the first slit was opened horizontally above 10 μm. The vertical fringe visibility was less sensitive to the vertical opening of slit 1, and good contrast was obtained with a 80 μm vertical opening. It is likely that the finite transverse coherence of the beam reduced the fringe contrast, since the transverse coherence lengths are approximately 13 and 500 μm in the horizontal and vertical direction, respectively, 20 m from the source at 3.1 keV (see Appendix *B* for definitions of coherence lengths).

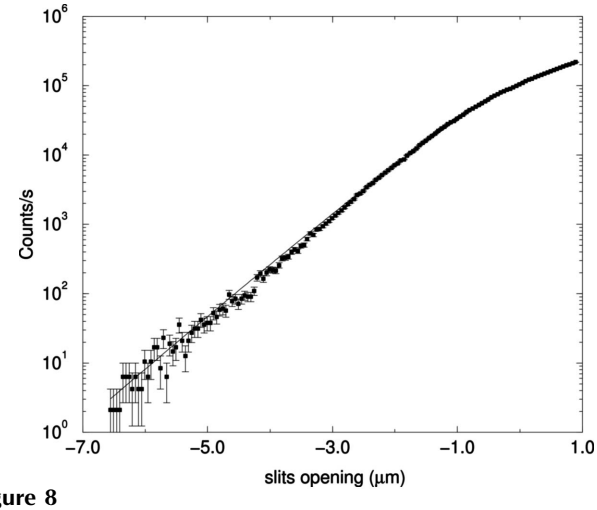

Figure 8
Measured transmission through a two-dimensional aperture *versus* the slit opening in one direction Δ. The two-dimensional aperture was opened by 100 μm in the other perpendicular direction. The solid line is a least-squares fit to the model described in the text.

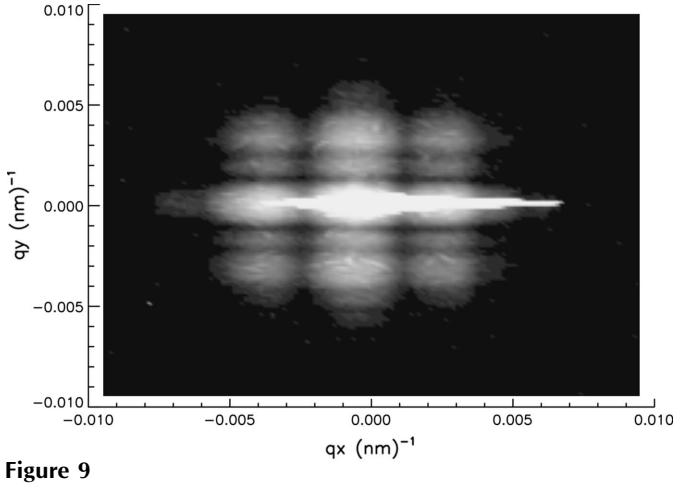

Figure 9
A 'phase peak' diffraction pattern of a 6 μm × 6 μm aperture generated with 3.1 keV X-rays.

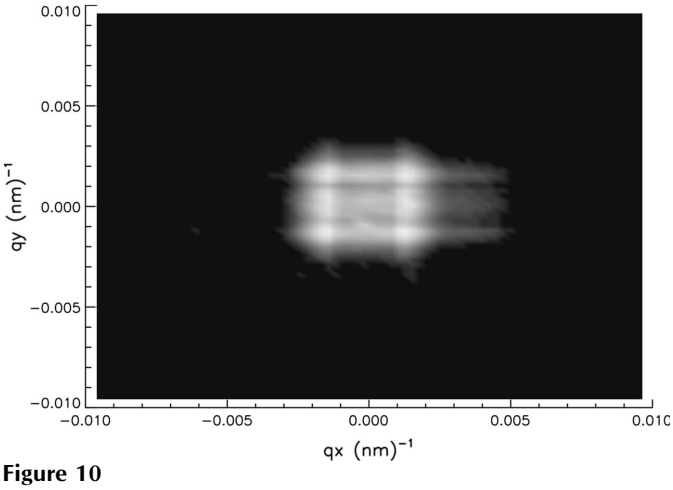

Figure 10
Diffraction pattern of a 6 μm × 6 μm aperture generated with 5.5 keV X-rays. Note the qualitative differences between this figure and Fig. 9

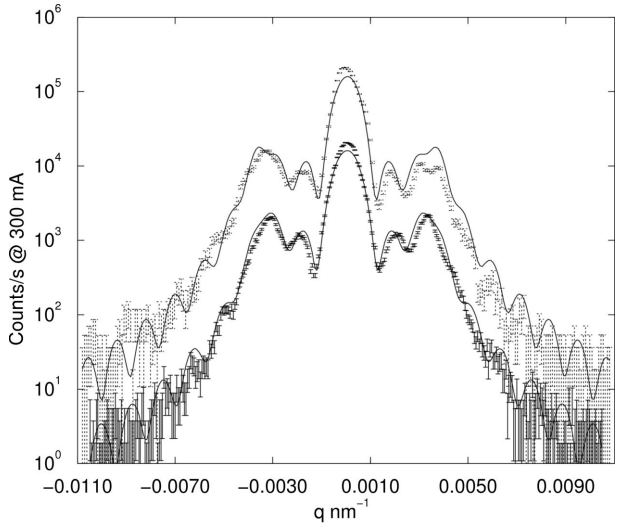

Figure 11
Diffraction patterns with the same opening as Fig. 9 measured with the PIN diode detector masked with a 20 μm × 20 μm GaAs aperture placed 950 mm behind the small aperture. (Bottom) Horizontal scan. The solid line is a least-squares fit to equation (3). (Top) Vertical scan multiplied by a factor of 10.

While keeping a fixed 6 μm × 6 μm aperture, we investigated the energy dependence of the diffraction pattern by setting the Si analyzer to various energies. Fig. 10 shows the diffraction pattern at 5.5 keV. Here the opening of slit 1 was 1 μm × 1 μm. For an infinitely absorbing edge ($\beta \rightarrow \infty$), the diffracted intensity is only dependent on the wavevector, and not on the energy of the X-rays used. Here, Figs. 9 and 10 are qualitatively quite different. For example, the peak intensity is not at $q = 0$ like in Fig. 10. The four phase peaks have the most intensity. Also, the position of the phase peak has moved to lower wavevector as expected since the magnitude of the phase peak position is inversely proportional to energy. Also, one notices that the diffracted intensity extends to higher wavevectors in Fig. 9 than in Fig. 10. This observation can be explained by the uncertainty principle because, as the energy increases, the effective slit opening increases, thus the extent of the diffracted intensity in reciprocal space is reduced. Finally, at higher energies the contribution of the field transmitted through the edges becomes the dominant contribution to the diffracted intensity, which explains the increase in intensity of the phase peak. These observations are consistent with Fig. 5.

To increase the dynamic range in the tails of the diffraction pattern, we measured the diffracted intensity with the PIN diode masked with a 20 μm square aperture. A vertical and a horizontal scan of the detector are shown in Fig. 11. We assumed that the error in the raw data followed Poisson statistics. The data were linearized with a 1.7 μs dead-time correction, and the error bars of the linearized signal were calculated from standard error analysis. The solid line is a least-squares fit of equation (3) convolved with the detector resolution, which yielded $\Delta = 5$ μm, $\theta = 50^\circ$ in the horizontal direction and $\Delta = 5.5$ μm, $\theta = 53^\circ$ for the vertical scan. We used the index of refraction shown in Table 1 at 3 keV. The qualitative agreement is excellent. The data and the fit fall rapidly with the same slope indicating that the diffracted intensity falls as expected as q^{-4}. The position of the fringes in the data and the fit agree fairly well for $|q| < 5 \times 10^{-4}$ Å^{-1}. The quantitative agreement can be improved if the coefficient of absorption β is varied in the fit. Then, the χ^2 of the resulting fit is reduced by a factor of two, resulting in a value of $\beta = 2.1 \times 10^{-5}$ and 2.5×10^{-5} for the horizontal and vertical scan, respectively. Apart from a possible underestimation of β, the quantitative difference between the fit and data may be explained in part by the fact that the inclination of both edges are difficult to align to better than 5°, thus they may be slightly different. The angle of incidence of the X-rays with respect to the plane of motion of the edges may also be off by a few degrees. An angular offset $\Delta\theta$ of 5° will move the phase peak in reciprocal space by $\Delta k/k_p \simeq (d\alpha/d\theta)\Delta\theta = 2\Delta\theta/\tan(2\theta) = 10\%$. This offset is comparable with the relative FWHM of the peak given by $\Delta k_p/k_p \simeq 2\beta/\delta = 31\%$ at 3 keV. It is also possible that some asymmetry in the pattern is caused by the fact that the two blades are not coplanar, an effect previously seen with roller-blade slits (Libbert *et al.*, 1997). Note also that a vertical angle–energy correlation is caused by the Si (111) analyzer, causing an energy spread of about 5 eV over the wavevector range shown in Fig. 11. This would affect the fit function through the index of refraction and wavelength.

The simple model derived in equation (3) assumes the same inclination for both edges, but, for a more careful quantitative test, one can generalize the treatment for two different orientations of the slit jaws. For a slit with two different inclination angles, one expects to observe two phase peaks at slightly different wavevectors. The Fourier amplitudes of the two slit jaws will also be different owing to different effective absorption lengths. As a first demonstration of this phase grating diffraction, the simple theory correctly accounts for the decay of the measured intensity $I(q)$ in the tails, for the position and presence of a phase peak, and for the energy dependence of $I(q)$. The diffraction pattern is also more symmetric and can be better controlled than the diffraction pattern of a typical laser-drilled pinhole shown in Fig. 1.

5. Discussion

In Appendix *B*, we discuss the material issues that control the absolute intensity of the parasitic scattering from inclined slit blades. For small-angle X-ray scattering experiments with coherent beams, one wants $1/(g\beta) < k_0 l_1/q_1 \simeq 2$ µm. Our results show that GaAs works well for soft X-rays near 3 keV since the fringe contrast was good. Near 8 keV, one would need to use heavier material such as highly polished Pt edges. At this energy for Pt, $\beta = 5.2 \times 10^{-6}$, $\delta = 5.3 \times 10^{-5}$ (Henke *et al.*, 1993), thus $\Delta k/k_p \simeq 20\%$. At an inclination angle $\theta = 80^\circ$, $1/(g\beta) \simeq 0.8$ µm, and $k_p = 1.2 \times 10^{-3}$ Å^{-1}. In Fig. 12, the theoretical parasitic count rate per speckle for a typical circular pinhole with a diameter of 5.6 µm is shown. The incident count rate is 10^{10} photons s^{-1} (25 µm^2)$^{-1}$. For our two-dimensional Pt aperture, two scans are shown, one along a direction parallel to the slit jaw motion and one at 45° from it. The circular pinhole area is set at 25 µm^2 in order to keep the same integrated flux on the sample. For the circular pinhole, we chose a speckle area equal to $\pi(2\pi/D)^2$.

A typical detector has a dark count rate ranging from 10^{-3} to 1 Hz. The background predicted by the Pt slit above about 6×10^{-3} Å^{-1} is much smaller than the tails of diffraction from the circular pinhole. Above approximately 3×10^{-2} Å^{-1}, the parasitic diffraction becomes smaller than the detector noise. The diagonal is the direction of steepest decay for these Pt slits, the tails of the diffraction pattern falling as $1/k^8$. For an incident flux of 10^{10} photons s^{-1} (25 µm^2)$^{-1}$, the parasitic count rate from the slit is 3 photons s^{-1} (speckle)$^{-1}$ at $k = 4 \times 10^{-3}$ Å^{-1}, and becomes negligible for wavevectors of interest in an XPCS experiment. These slits could reduce the background when compared with a circular aperture. They are well suited for weak scattering samples using a detection scheme that uses a single-channel photon-counting detector coupled to a digital correlator. Their diffraction pattern though is energy dependent, thus the slit geometry adds complications to the experimental design.

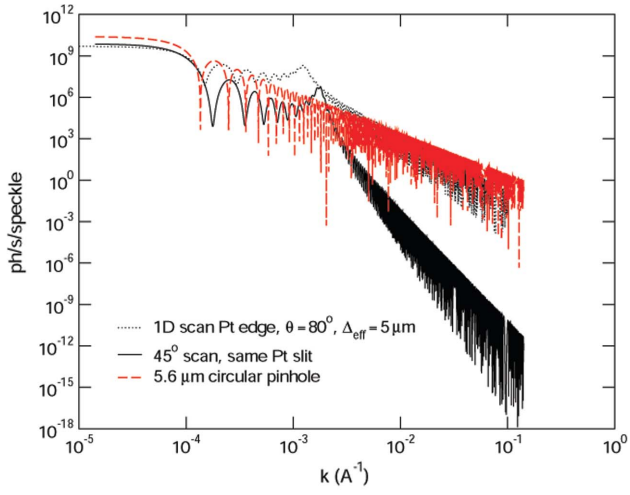

Figure 12
Theoretical parasitic count rate per speckle for a 5.6 µm-diameter pinhole (dashed) and a two-dimensional Pt aperture with $\theta = 80^\circ$ and $\Delta_{\mathrm{eff}\,x} = \Delta_{\mathrm{eff}\,y} = 5$ µm at 8 keV. For the Pt aperture, two scans are shown, one along a direction parallel to the diagonal of the aperture (solid), and one along the direction of the blade motion (dotted).

We believe that the stray scattering observed when using standard X-ray diffraction slits can be explained in part by refraction effects described in our model. The theory derived here applies for all slit jaws with $\gamma = 90^\circ$, and is present for an ideal atomically flat edge. Even with an ideal edge, misalignment of the order of 1° or less (see Fig. 4) with respect to the main beam will give rise to a phase peak.

In practice, it may be difficult to rely on cleaved edges to provide an ideal blade. It would be interesting to develop either with modern deposition techniques or by lithography more complicated absorption profiles which could produce say a Gaussian absorption profile. Significant progress has been made in recent years in producing parabolic absorption profiles to produce refractive lenses.

Note that these slits can be of general use in incoherent small-angle X-ray scattering experiments because their tails fall much faster than standard slits. For example, although GaAs edges are not good for coherent small-angle scattering at 9 keV because $1/(g\beta) > l_t$, they may be useful to use as slits in incoherent SAXS experiments, where the slit opening does not need to be kept smaller than the transverse coherence length. The fast decay of $I(q)$ in Fig. 5 for 9 keV X-rays could be advantageous in SAXS experiments. Note also that inclined GaAs slits could be well suited for experiments in the UV and soft X-ray range because the phase peak can be suppressed when $\delta < \beta$, which occurs in this energy range.

In conclusion, we have designed new slits which use an apodization technique to reduce the parasitic background caused by the Fraunhofer diffraction pattern of the aperture in a coherent SAXS experiment. Using inclined cleaved GaAs edges, we observed a peculiar 'phase peak' diffraction pattern which we explained using a theory that takes into account both the absorption and phase delay that occurs in the blade. As opposed to the diffraction pattern of a circular pinhole, the diffraction pattern of these slits for a fixed opening is strongly energy dependent. As predicted, the phase peak wavevector is inversely proportional to energy. The model proposed describes the data well.

APPENDIX *A*
Slit assembly

The slit blades are mounted on ball-bearing slides (Part No. PB04-05) purchased from Precision Industrial Components Design Corp., Middlebury, CT, USA. In a recent experiment we found that the maximum pitch angle of these slits is about a few milliradians for a range of travel of a millimeter or so, thus the motion of these slits keep their alignment fixed to a few milliradians. The DC motors were purchased from MicroMo Electronics Inc., Clearwater, FL, USA. We used the motor model 1016M012GK380 with encoder HEM1016M10 and either a 256:1 or 1024:1 gear ratio. From the manufacturer specification, some shaft play exists which can cause backlash. These motors should be ordered with the reduced shaft play option.

APPENDIX *B*
Estimates of parasitic background in a coherent SAXS experiment

In order to use the inclined slits in an XPCS experiment, several conditions should be considered which minimize the parasitic scattering from the slit diffraction pattern and preserve the coherence. The diffracted intensity for a two-dimensional aperture made with two perpendicular slits with inclined edges is $I(k_x,k_y) = \Phi i(k_x) i(k_y)/(2\pi)^2$, where Φ is the photon flux in photons s^{-1} μm^{-2}, $i(k)$ is the function on the right-hand side of equation (3), and the $(2\pi)^2$ factor ensures that the integral over reciprocal space of $I(k_x,k_y)$ is equal to $\Phi\Delta_{\mathrm{eff}x}\Delta_{\mathrm{eff}y}$. Here $\Delta_{\mathrm{eff}x}$ and $\Delta_{\mathrm{eff}y}$ are the effective openings in the horizontal and vertical directions. In a SAXS experiment, we want to minimize the parasitic diffracted count rate accepted in the detector solid angle. In an XPCS experiment, to observe a speckle with sufficient contrast, the detector resolution must be kept below the speckle size $\Delta k \simeq 2\pi/\Delta_{\mathrm{eff}}$. If we set the resolution as the speckle size, the parasitic count rate in the detector is approximately

$$N(k_x, k_y) = \frac{\Phi i(k_x) i(k_y)}{\Delta_{\mathrm{eff}x}\Delta_{\mathrm{eff}y}}, \qquad (6)$$

where N is measured in photons s^{-1} since $i(k) \simeq 1/g^2$ in equation (3). In equation (6), we approximated the convolution of the detector resolution and $I(k_x,k_y)$ as the product of the two. This approximation gives a good estimate of the parasitic count rate, although it does not cause any smearing of the fringes owing to the finite resolution.

To minimize $N(k_x,k_y)$ in the range of the wavevector of interest in a small-angle XPCS experiment (10^{-1} Å^{-1} > k > 4×10^{-3} Å^{-1}), one wants the phase peak position $k_{\mathrm{p}} \ll 4 \times 10^{-3}$ Å^{-1}. Also, one should choose a material such that the parasitic count rate at the phase peak $N(k_{\mathrm{p}},k_{\mathrm{p}})$ is as small as possible. To illustrate the material aspect in this optimization problem, we first consider the case of closed slits, where $\Delta_{\mathrm{eff}} = 1/(g\beta)$. From equation (3), one can show that

$$N(k_p, k_p) \simeq \frac{\Phi(\beta^2+\delta^2)^2}{g^4\beta^4\delta^4\Delta_{\mathrm{eff}x}\Delta_{\mathrm{eff}y}} = \frac{\Phi(1+\beta^2/\delta^2)^2}{g^2\beta^2}. \qquad (7)$$

For hard X-rays, since $\beta/\delta \ll 1$, the parasitic count rate is minimized when the inclination factor α and the linear absorption coefficient of the material (proportional to $k_0\beta$) are large. When the slits are opened, the parasitic count rate $N(k_{\mathrm{p}},k_{\mathrm{p}}) \simeq \Phi/(g^4\beta^4\Delta_{\mathrm{eff}x}\Delta_{\mathrm{eff}y})$ will be smaller than $\Phi/(g\beta)^2$; therefore equation (7) represents an upper limit for the parasitic background.

Another material aspect to recall is that the ratio $\Delta k/k_{\mathrm{p}} \simeq 2\beta/\delta$, the FWHM of the phase peak, is only material dependent. From data from Table 1 for GaAs at 3 keV, $\Delta k/k_{\mathrm{p}} = 31\%$. Provided that the phase peak is at a wavevector well below the range of the wavevector probed in the experiment, $N(k_x,k_y)$ will be much smaller than the phase peak intensity. For monoatomic material with an atomic number Z, one can show that at an energy E between the K and L edges for example, or above the K edge of the slit material, the ratio $\delta/\beta \propto E^2/Z^3$ (Als-Nielsen, 1993). Choosing a high-Z material ensures that refraction is reduced with respect to absorption, although it increases the width of the phase peak.

For the wavevector of interest in an experiment with $|k_x - k_{\mathrm{p}}|$ and $|k_y - k_{\mathrm{p}}| \gg 2g\beta$, when we neglect the oscillatory terms in equation (3), the diffracted count rate becomes approximately equal to

$$N(k_x, k_y) \simeq N(k_p, k_p)(k_p^2/k_x k_y)^4 \simeq \Phi(1+\delta^2/\beta^2)^2\left[g\delta/(k_x k_y)\right]^4/(\Delta_{\mathrm{eff}x}\Delta_{\mathrm{eff}y}). \qquad (8)$$

To minimize the parasitic signal, one would choose a material with a large Z to reduce the ratio δ/β, and would keep the phase peak wavevector below approximately 10^{-3} Å^{-1}. Since $k_{\mathrm{p}} \propto 1/E$, larger energies also help to reduce the parasitic diffraction from the slit.

The signal-to-noise ratio in an XPCS experiment depends not only on the parasitic background discussed above but also on the transverse and longitudinal illumination of the sample. For the transverse coherence to be preserved, the effective slit opening $\Delta_{\mathrm{eff}} = \Delta + 1/(g\beta)$ must be smaller than the smallest transverse coherence length of the source. For an incoherent source with a Gaussian spatial profile, one can show using the Van Cittert–Zernicke theorem that the transverse coherence length is $\lambda R/(2\pi^{1/2}\sigma)$ (Goodman, 1985; Dierker, 1997). At the APS, the source is currently 25 times wider horizontally than vertically, thus the transverse coherence length is smallest in the horizontal direction. For the APS, the horizontal r.m.s. source size $\sigma_x \simeq 300$ μm, therefore the horizontal transverse coherence length will be approximately 5.4 μm near 8 keV at a distance $R = 40$ m from the source. For small-angle XPCS measurements, one wants to observe good contrast up to wavevectors around $q_{\mathrm{l}} = 2 \times 10^{-2}$ Å^{-1}. In order to preserve the contrast, the aperture may have to be closed to its smallest setting $1/(g\beta)$ to minimize the optical path difference, so $1/(g\beta)$ should be made smaller than $k_0 l_{\mathrm{l}}/q_{\mathrm{l}} \simeq 2$ μm. For controlling both the transverse and longitudinal coherence, one should choose a material and inclination angle such that $1/(g\beta) <$ 1 μm at 8 keV.

We thank Professor Roy Clarke for providing the thin GaAs wafers. We thank James Stathis, Mason Okubo and Ramin Ershadi from Newport Corp. for lending us an MM3000 controller and for their advice on the operation of the MM3000. The excellent technical support from Rick Greene and Tony Lenhard was greatly appreciated. EMD acknowledges the support of the Natural Science and Engineering Council of Canada. This work was supported by a National Science Foundation Grant No. DMR-92-17956, and the NSLS is operated under a US Department of Energy contract No DE-AC02-98CH10886.

References

Als-Nielsen, J. (1993). *Neutron and Synchrotron Radiation for Condensed Matter Studies, Volume I: Theory, Instruments and Methods*, edited by J. Barushel, J. Hodeau, M. Lehmann, J. Regnard and C. Schlenker, p. 25. Paris: Les Editions de Physique Springer-Verlag.

Berman, L., Yin, Z., Dierker, S., Dufresne, E., Mochrie, S., Tsui, O., Burley, S., Shu, F., Xie, X., Capel, M. & Sweet, R. (1997). *Synchrotron Radiation Instrumentation: Tenth US National Conference*, edited by E. Fontes, Vol. 417, pp. 71–79. College Park: American Institute of Physics.
Born, M. & Wolf, E. (1970). *Principles of Optics.* Oxford: Pergamon.
Brauer, S., Stephenson, G., Sutton, M., Brüning, R., Dufresne, E., Mochrie, S., Grübel, G., Als-Nielsen, J. & Abernathy, D. (1995). *Phys. Rev. Lett.* **74**, 2010–2013.
Dierker, S. (1997). *Light Scattering and Photon Correlation Spectroscopy, Proceedings of a NATO Advanced Research Workshop*, edited by E. Pike. Dordrecht: Kluwer Academic.
Dierker, S., Pindak, R., Fleming, R., Robinson, I. & Berman, L. (1995). *Phys. Rev. Lett.* **75**, 449–452.
Dufresne, E. M., Nurushev, T. S., Dierker, S. & Clarke, R. (2002). *Phys. Rev. E*, **65**, 061507.
Goodman, J. (1985). *Statistical Optics*, 1st ed. New York: John Wiley.
Henke, B., Gullikson, E. & Davis, J. (1993). *Atom. Data Nucl. Data Tables*, **54**, 181–342.
Libbert, J. L., Pitney, J. A. & Robinson, I. K. (1997). *J. Synchrotron Rad.* **4**, 125–127.
Livet, F. (2007). *Acta Cryst.* A**63**, 87–107.
Michette, A. G. & Buckley, C. (1993). Editors. *X-ray Science and Technology.* Bristol: Institute of Physics Publishing.
Nikulin, A. & Davis, J. (1998). *Opt. Commun.* **155**, 231–235.
Stefan, P., Krinsky, S., Rakowsky, G. & Solomon, L. (1995). *Proceedings of the 1995 Particle Accelerator Conference*, Vol. 4, pp. 2435–2437. New York: IEEE.
Veen, J. F. van der, Riemersma, A. J., Schlatter, H., Abernathy, D. L. & Grübel, G. (1997). *J. Synchrotron Rad.* **4**, 64–66.
Vlieg, E., De Vries, S. A., Alvarez, J. & Ferrer, S. (1997). *J. Synchrotron Rad.* **4**, 210–213.
Xiao, X., de Jonge, M. D., Zhong, Y., Chu, Y. S. & Shen, Q. (2006). *Opt. Lett.* **31**, 3194–3196.